PAPER

Check for updates

Operando X-ray absorption spectroscopy of a Pd/γ-NiOOH 2 nm cubes hydrogen oxidation catalyst in an alkaline membrane fuel cell†

Maria Alesker,[a] Istvan Bakos,[b] Veronica Davies,[c] Qingying Jia, (iD)[c] Luba Burlaka,[a] Valeria Yarmiayev,[a] Anya Muzikansky,[a] Anna Kitayev,[ad] Miles Page,[d] Sanjeev Mukerjee[c] and David Zitoun (iD) *[a]

A fundamental understanding of the hydrogen oxidation reaction (HOR) mechanism requires the synthesis of model catalysts with designed surfaces, and advanced characterization techniques of the active sites. Although HOR are fast under acidic conditions, HOR kinetics are sluggish under alkaline conditions, even on platinum group metals (PGMs). Herein, we propose the use of an effective high-surface-area carbon supported Pd/γ-NiOOH HOR electrocatalyst, made from organometallic precursors. The enhanced activity, provided by nickel oxy-hydroxide (γ-NiOOH) 2 nm nanocubes, was confirmed experimentally in an alkaline exchange membrane fuel cell. Contrary to previous reports, the phase and crystallographic orientation of the γ-NiOOH nanocubes (<2 nm in size) were fully ascribed through high-resolution transmission electron microscopy. *Operando* X-ray absorption spectroscopy revealed a redox behavior of Pd and Ni during the electrocatalysis. Each phase has an attributed role in the mechanism, *i.e.*, hydrogen binding to the Pd metal and hydroxide binding to the γ-NiOOH, confirming the theory and experiments observed with bimetallic structures.

1. Introduction

The development of anion-exchange membrane fuel cells (AEMFCs) has stressed the need for efficient HOR electrocatalysts.[1–4] In alkaline medium, the HOR activity of PGM catalysts (Pt, Ir, and Pd) is reduced by almost two orders of magnitude compared to the activity in acidic medium.[5–8] However, multi-metallic systems demonstrate a high electrocatalytic activity, as shown on alloyed IrPdRu/C, and compared to Ir/C and Pt/C.[9] The studies on single crystalline surfaces reveal the enhancement in HOR activity when the surfaces are doped with alkaline or transition metal cations or clusters, directly deposited on the single crystalline sur-

faces or on the surface of bimetallic alloys.[10,11] The studies are specifically relevant to alkaline medium, where the stability of earth-abundant hydroxide species enables the addition of non-PGM catalysts or their sole use,[1,12–15] as reported in a recent review on HOR in alkaline medium.[16] Although the hydrogen binding energy of palladium is very close to the platinum one,[17,18] palladium HOR electrocatalysts have not been extensively reported because of the high experimental overpotential of pure Pd catalysts, even though multi-metallic electrocatalysts containing Pd should show a great improvement. Indeed, the partial coverage of Ni thin films with Pd has shown that bimetallic Ni–Pd surfaces are much more active than pure Pd for HOR in an alkaline solution.[19] This approach has been implemented on a bimetallic electrocatalyst in an AEMFC, leading to a 5 fold better Pd utilization.[20] In that work, the decoration of commercial nanoscale Ni was achieved from a rapid reduction of aqueous Pd(ii) complexes with hydrides, and as a result, the nanostructure was poorly defined. On the other hand, the use of organometallic compounds as metallic precursors has yielded alloys[21] or core–shell structure with high HOR activity,[22] these reaction processes are typically at low temperature[23,24] with short reaction time.[25] In all the previous reports, the structures were bimetallic with no evidence for an oxide or hydroxide phase. It is however well recognized with studies on extended surfaces

[a] *Department of Chemistry, Bar Ilan Institute of Technology and Advanced Materials (BINA), Bar Ilan University, Ramat Gan, 52900, Israel. E-mail: david.zitoun@biu.ac.il*

[b] *Institute of Materials and Environmental Chemistry, Hungarian Academy of Sciences, Budapest, Hungary*

[c] *Department of Chemistry and Chemical Biology, Northeastern University, Boston, MA 02115, USA*

[d] *PO-CellTech Ltd., Hatochen 2, Caesarea Business and Industrial Park, Caesarea, 30889 Israel*

† Electronic supplementary information (ESI) available: Additional TEM and HRTEM images. See DOI: 10.1039/d0cy01815e

This journal is © The Royal Society of Chemistry 2021

Catal. Sci. Technol., 2021, **11**, 1337–1344 | **1337**

that metal hydroxide species plays an important role in promoting HOR in alkaline medium. In parallel to the Pd/Ni system, Pd/CeO_2 has also been extensively studied and has shown the critical role of the palladium–ceria interface on the HOR activity.[26–30]

In the present study, we investigate the alkaline HOR of biphasic Pd/γ-NiOOH supported on carbon. The slow decomposition of organometallic complex $Ni(COD)_2$ yields 2 nm γ-NiOOH nanocrystals with a cubic shape on the surface of nanoscale Pd. This catalyst was tested as an HOR electrocatalyst in alkaline medium and the *operando* X-ray absorption spectroscopy (XAS) was collected on both the Pd and Ni K edges simultaneously for structural characterization at the atomic scale during the HOR.

2. Experimental methods

2.1 Synthesis

Materials. $Ni(COD)_2$ (STREM, 98%) was stored in a freeze of a glovebox at −20 °C and used as received.

C/Pd 20% w/w (Premetek), tetrahydrofuran (Acros, 99.5%).

Synthesis of C/Pd@Ni nanocrystals. $Ni(COD)_2$ (0.85 mmol) was dissolved in tetrahydrofuran (20 mL) with the subsequent addition of C/Pd nanopowder (400 mg) in the inert atmosphere of a glovebox. After addition of 50 ppm water in 5 mL tetrahydrofuran, the reaction proceeded overnight under nitrogen at room temperature under constant stirring. The products were separated *via* centrifugation and redissolution in tetrahydrofuran.

2.2 Structural characterization

HRTEM study was carried out at 200 kV on a JEOL JEM-2100 (LaB6) TEM. Fast Fourier transform (FFT) analysis of HRTEM images was used for structural analysis. HRTEM images and EDX measurements were obtained at 200 kV on a JEOL JEM-2100F TEM. The crystalline phases and crystallinity of the prepared powders of the final products were determined using XRD with Cu Kα (0.1541 nm) radiation (Rigaku SmartLab).

2.3 Electrochemical measurements

Single-compartment PFTE cell was used in order to avoid the effect of impurities dissolving from glass components. The cell was equipped with two reference electrodes: (i) a Pt/Pt which was used in hydrogen saturated solutions (as hydrogen electrode); (ii) a palladium wire, filled up electrolytically with hydrogen in a separate cell before the experiments. The latter was used as a reference in H_2-free Ar saturated solutions. All potentials quoted are on RHE-scale. A glassy carbon rod served as a counter electrode. Hydrogen of 99.999% purity was used in the HOR experiments and 99.9995% purity argon was used as an inert gas. The catalyst loading on the glassy electrode was 5 μg. The alkaline solution was prepared from KOH (Sigma-Aldrich, 99.998%) and ultrapure water. The glassy carbon was mounted on a rotating electrode. Poten-

tials were corrected for ohmic losses, measured by impedance spectroscopy before each polarization curve. After purging in Ar, the voltammograms were collected at 100 mV s^{-1} from 0.05 to 1.35 V *vs.* RHE. Cathodic polarization curves were recorded after saturation of the solutions with H_2 by sweeping from 0.6 V to 0 V *vs.* RHE at 20 mV s^{-1} using different rotating speeds (225, 400, 625, 900, 1225 rpm).

2.4 Fuel cell measurements

The as-prepared C/Pd/γ-NiOOH and commercial (Premetek, Inc.) Pd/C anode catalyst was tested in a 5 cm^2 fuel cell (Fuel Cell Technologies, AZ, USA). Catalyst-coated membranes (CCMs) for AEMFCs were prepared with low loadings of 0.4 mg cm^{-2} for the Pd/γ-NiOOH, and loading of 0.5 mg cm^{-2} for Pd as the anode catalysts. Cathode catalyst layers were prepared according to the procedure described in ref. 20, with previously reported Ag-based catalyst (Quantum Sphere Inc.) at loading 3 mg cm^{-2}.[31] Catalyst inks were prepared by mixing the dispersed catalyst in a solution of a quaternary ammonium-functionalized ionomer (IEC 2.4 ± 0.2 mmol g^{-1}) and applied onto an anion exchange membrane (IEC = 2.0 ± 0.2 mmol g^{-1}; s = 43 ± 5 mS cm^{-1}, OH$^-$/80 °C/92% RH; t = 30 ± 2 mm; liquid water uptake 90 ± 15% at 20 °C) as reported previously.[31]

The AEMFC tests were performed at the cell temperature of 73 °C, with dry H_2 on the anode side, at 0.2 standard liter per minute (sLPM), room temperature, 4 bar$_{abs}$, and humidified CO_2-free air on the cathode side, at 1 sLPM, 100% RH, 2 bar$_{abs}$. Polarization curves were taken at scan rate 100 mV min^{-1}, after the fuel cell reached steady current at 50 mV.

2.5 *Operando* X-ray spectroscopy

The preparation method of the XAS electrodes can be referred to our previous work.[32] The final Pd geometric loadings were chosen to give 0.5 transmission spectra edge heights at the Pd K-edge. The XAS experiments were conducted at room temperature in a previously described flow half-cell[32] in which continuously H_2-purged 0.1 M KOH was circulated. The voltage cycling limits were 0 to 0.54 V$_{RHE}$. The XAS spectra at the Pd and Ni edges were collected in the transmission and fluorescence modes, respectively, at the beamline 2-2 at the Stanford Synchrotron Radiation Lightsource (SSRL), SLAC National Accelerator Laboratory. Typical experimental procedures were utilized with details provided in our previous work.[33]

3. Results and discussion

The standard catalyst is a commercial Pd supported catalyst (20% wt on C). After dispersion in dry THF, the synthesis proceeds through the slow decomposition of zerovalent organometallic precursor $Ni(COD)_2$ at room temperature overnight. Upon addition of 50 ppm of water, the complex undergoes slow hydrolysis and the yellowish solution turns transparent after filtration of the catalyst. The resulting nanocrystals have
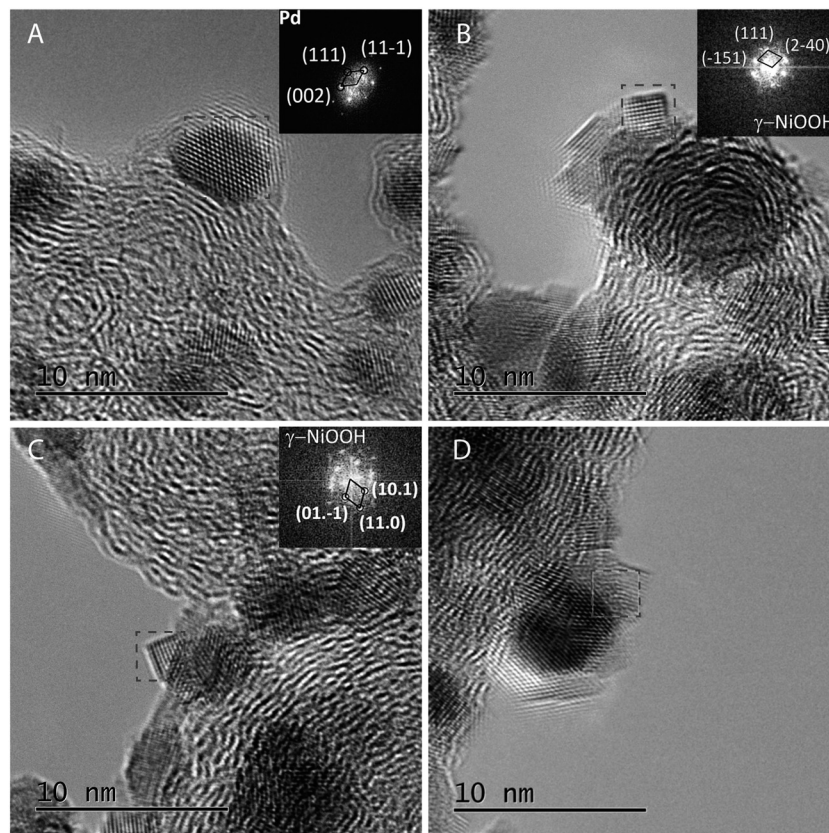
1338 | *Catal. Sci. Technol.*, 2021, **11**, 1337–1344

This journal is © The Royal Society of Chemistry 2021

Fig. 1 High-resolution transmission electron microscopy (HR-TEM) of the Pd and Pd/γ-NiOOH samples: (A) pristine Pd samples with fast-Fourier transform (FFT) (inset); (B–D) HRTEM images of Pd/γ-NiOOH with corresponding FFT (insets).

been analyzed by TEM (Fig. S1†) and high-resolution TEM (HR-TEM) (Fig. 1 and S2 and S3†). The pristine catalyst consists of single-crystalline Pd nanoparticles well dispersed on carbon (Fig. 1A). The Pd crystallizes in the face-centered cubic system (JCPDS # 05-0681; $Fm\bar{3}m$) and the nanocrystals do not display a specific crystallographic orientation. After the reaction, the Pd nanocrystals are covered with cubic shape nanocrystals with a 2 nm average size (Fig. 1B). The nucleation of the new phase occurs selectively on the surface of Pd and no nickel content could be found anywhere else (Fig. S4†). The nanocrystals crystallize in a hexagonal phase corresponding to γ-NiOOH, commonly named as nickel oxy-hydroxide. The γ-NiOOH nanocubes follow the orientation of the underlying Pd nanocrystals in most of the cases (Fig. 1B), while in a few occurrences, the cube edges have a 45° angle relative to the Pd surface, which gives them the appearance of a pyramid (Fig. 1C). Some of the Pd nanoparticles appear to be fully covered with NiOOH resulting in the observed core–shell structure in Fig. 1D.

The stoichiometry of oxygen and the Pd/Ni ratio is confirmed by EDX analysis (atomic ratio Pd : Ni : O ∼ 1 : 1 : 2). A careful analysis of the TEM pictures gives a particle size distribution of 4.0 ± 0.8 nm for the pristine Pd nanocrystals and 4.4 ± 0.9 nm for the Pd/γ-NiOOH nanoparticles (Fig. 2A). The powder X-ray diffraction (PXRD) reveals the presence of Pd crystalline phase with lattice constants that are close to FCC

Pd (JCPDS # 05-0681; $Fm\bar{3}m$, a = 3.8902 Å: blue lines), without any evidence of γ-NiOOH phase. The absence of γ-NiOOH phase on the PXRD can be explained by the small particle size of γ-NiOOH cubes (∼2 nm), even if the atomic ratio between the two phases is roughly 1 : 1 (Fig. S4†).

The electrocatalytic activity has been tested under alkaline conditions (0.1 mol L^{-1} KOH). The glass free electrochemical cell was used in conjunction with a working rotating glassy carbon electrode, a glassy carbon counter-electrode and a reversible hydrogen electrode (RHE), in order to avoid any Pt contamination. Cyclic voltammetry (CV) was recorded under Ar after prolonged deoxygenation and stabilization. The potential was scanned between 0.05 and 1.35 (or 1.5 V). Fig. 3A shows the cyclic voltammetry with the hydrogen and oxygen adsorption/desorption at potential typical of Pd. The electrochemical surface area (ECSA) was measured from the cathodic peak at 0.65 V/RHE, which is related to the reduction of oxygen species on Pd. The ECSA decreases from 122 m^2 g^{-1} for pristine Pd to 98 m^2 g^{-1} for Pd/γ-NiOOH, revealing the coverage of 20% of the Pd surface by γ-NiOOH. The 1 : 1 ratio between Pd and γ-NiOOH surface deduced from the Ni(II)/Ni(III) redox reaction is consistent with cubic γ-NiOOH nanocrystals, one facet of the cube sitting on the Pd surface, while the 5 facets left are exposed to the electrolyte.

The hydrogen oxidation reaction (HOR) activity was recorded in an H$_2$-saturated solution at T = 298 K. The
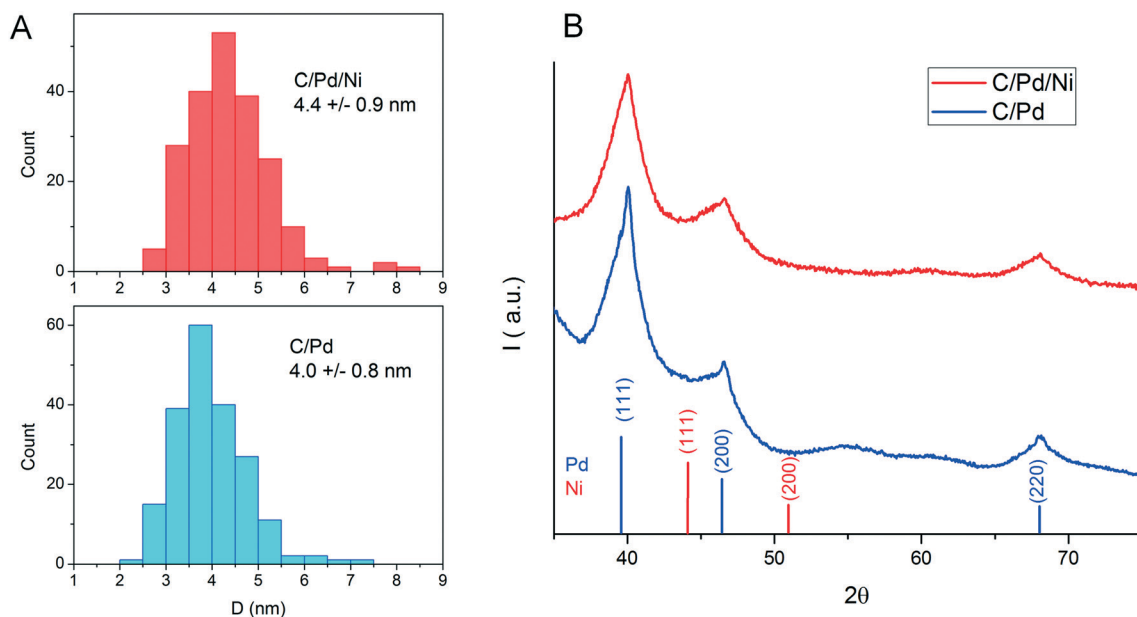
Fig. 2 (A) Particle size distribution (PSD) and (B) powder X-ray diffraction (PXRD) patterns of the catalysts (Pd and Ni reflections marked by solid lines).

cathodic polarization curves are shown in Fig. 3B to discard the hydrogen absorption in Pd. Pristine Pd catalyst shows very sluggish HOR activity and reaches the half-wave potential at 0.32 V *vs.* RHE. On the other hand, Pd/γ-NiOOH displays a much higher HOR activity with a half-wave potential at 0.05 V *vs.* RHE. The exchange current density (i_0) was calculated from the Tafel plots extracted from the plot of Nernstian overpotential (η_d) *vs.* kinetic current (i_k) as shown in Fig. 3C, and it reaches 0.2 mA cm$^{-2}_{Pd}$, a 10-fold increase compared to the pristine Pd catalyst, 0.02 mA cm$^{-2}_{Pd}$. Although part of the Pd active sites towards hydrogen is covered with γ-NiOOH (20% of the surface) and ECSA is lower, the mass activity at 0.1 V of the catalyst reaches 300 mA mg$^{-1}_{Pd}$, a value 5 times higher than pristine Pd. We interpret this phenomenon by "bifunctionality" of Pd/γ-NiOOH catalyst, and proximity of hydroxyl (OH) species to adsorbed hydrogen sites.[20] The hydroxyl species, provided by the γ-NiOOH nanocubes, promote high rate oxidation of the hydrogen atoms adsorbed on Pd surface, and therefore higher overall activity compared with Pd-only HOR catalyst.

The enhanced activity relative to pristine Pd is also demonstrated in an alkaline membrane fuel cell anode. Membrane-electrode assemblies (MEAs) were fabricated according to an already reported method,[20] with an anode Pd loading of 0.5 mg cm^{-2} for Pd, and 0.4 mg cm^{-2} for the Pd/γ-NiOOH anode catalyst. The fuel cell tests were carried out at 73 °C, also following a reported procedure.[20]

Fuel cell polarization curves (Fig. 4) show that a membrane-electrode assembly with an anode utilizing γ-NiOOH-decorated Pd electrocatalyst displays very strong activity enhancement *versus* a neat Pd-based electrocatalyst in an otherwise identical MEA. The performance in the MEA of the present catalyst material overcomes the previously

reported Ni/Pd catalyst,[20] where Pd was deposited on a commercial nickel nanopowder (also displayed in Fig. 4), suggesting that the presence of nickel surface hydroxide/oxyhydroxide species (rather than a clean Ni surface or local Ni–Pd alloying) likely also caused the reported activity enhancement *versus* Pd.

To elucidate the promotional role of γ-NiOOH for the HOR in alkaline medium, *operando* X-ray absorption spectra were collected at both Pd and Ni edges within the HOR potential region of 0.1–0.54 V in an H$_2$-saturated 0.1 M KOH electrolyte. As seen in Fig. 5a, the X-ray absorption near-edge structure (XANES) spectra of the Pd K-edge remained unchanged within the potential range of 0.1–0.54 V, and closely resemble that of the Pd reference foil. These results indicate that the Pd is in the reduced form of Pd^0 during the HOR. This is further confirmed by the extended X-ray absorption fine structure (EXAFS) fitting (Fig. 5b and c), which literally shows a pure metallic phase with the first shell Pd–Pd bond distance equal to that of the Pd foil (Table 1). The Pd–Pd coordination number of 10.3 ± 0.5 matches the particle size of 4.4 ± 0.9 nm as estimated by TEM. It is noted that the Pd–Ni interaction was not observed from the Pd perspective; neither was it seen from the Ni perspective. The Fourier transform of the EXAFS spectra collected at the Ni K-edge and the corresponding EXAFS fitting show that the Ni is predominantly in the form of Ni(II)oxide (Fig. 5e and f). The lack of Pd–Ni interactions from both the Pd and Ni perspectives safely rules out the hydrogen binding energy model wherein the Ni indirectly improves the HOR activity of Pd *via* optimizing the Pd–H binding energy. Interestingly, the intensity of the XANES spectra at the Ni K-edge, which arises from the forbidden transition 1s–3d (but allowed for by the p–d orbital hybridization), increases with increasing potential (Fig. 5d), indicating
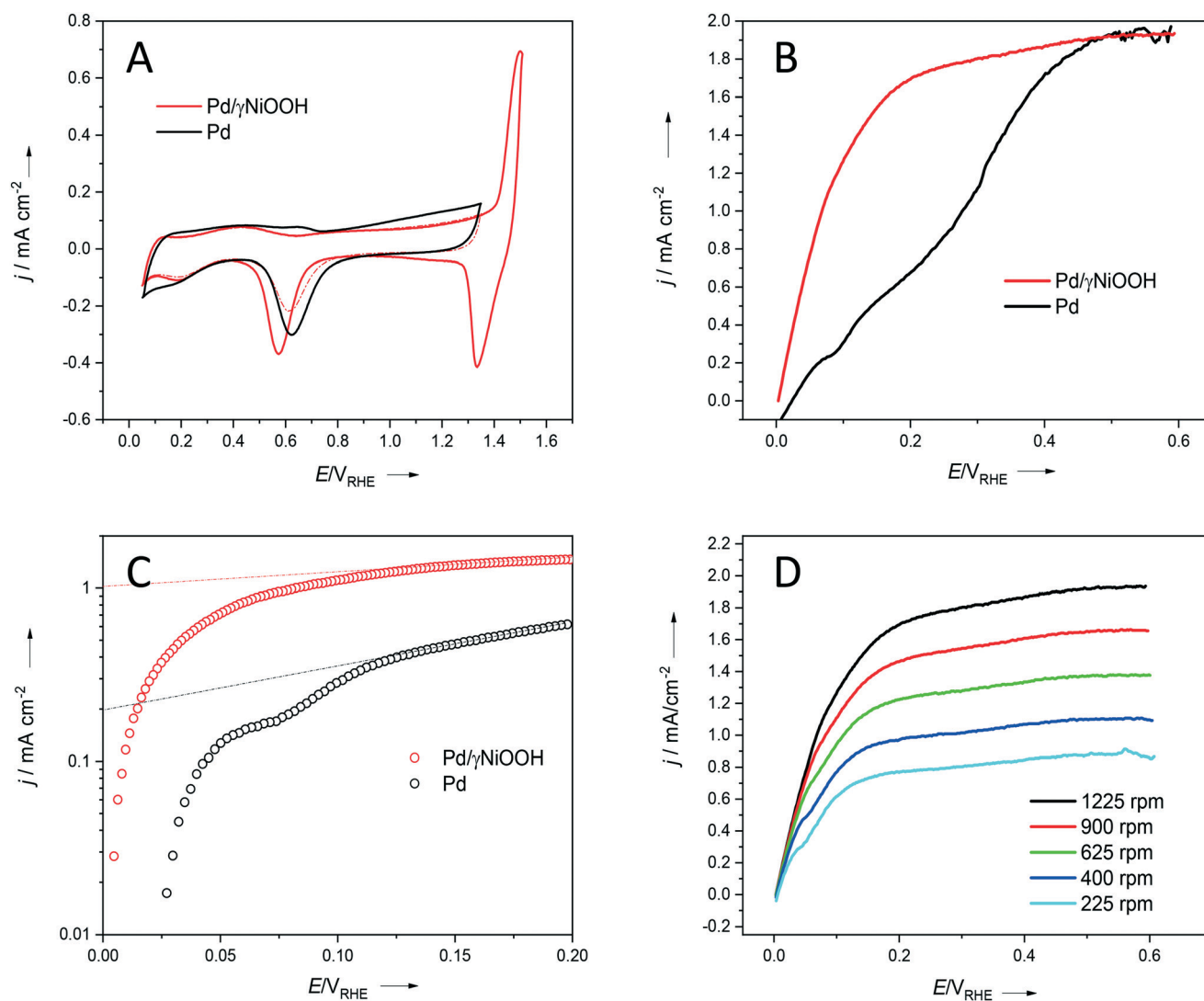
1340 | *Catal. Sci. Technol.*, 2021, **11**, 1337–1344

This journal is © The Royal Society of Chemistry 2021

Fig. 3 (A) Cyclic voltammograms recorded at 298 K in an Ar-saturated 0.1 M KOH solution; (B) ohmic loss corrected cathodic polarization at 298 K in an H_2-saturated 0.1 M KOH solution at 1225 rpm; (C) corresponding Tafel plot and (D) Pd/γ-NiOOH at different rotation speeds.
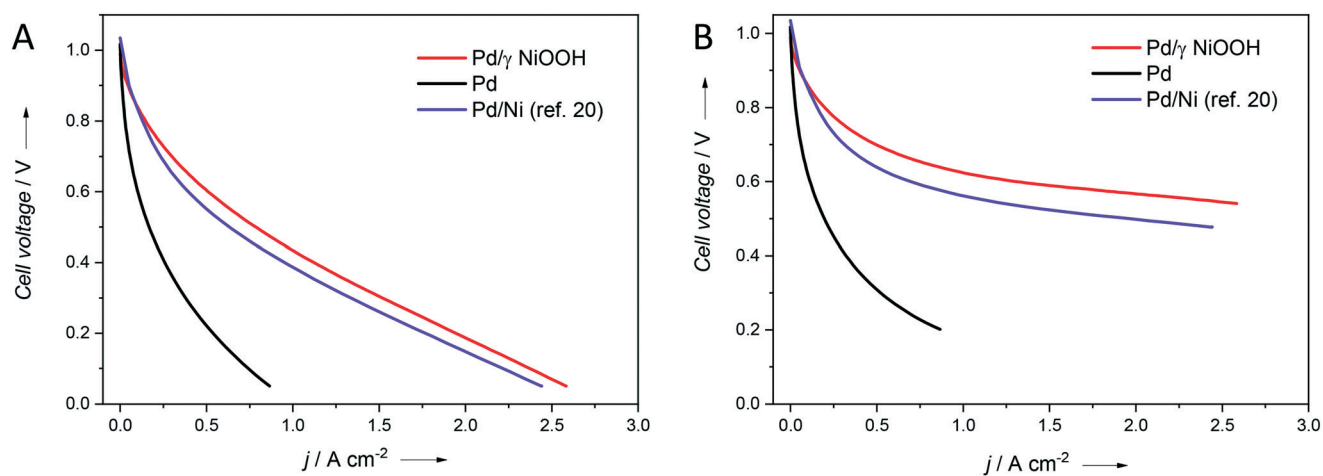

Fig. 4 (A) Raw and (B) IR-corrected polarization curves of MEAs with different anode catalysts, Pd/γ-NiOOH (red), Pd (black) and Pd/Ni composite from ref. 20 (purple).
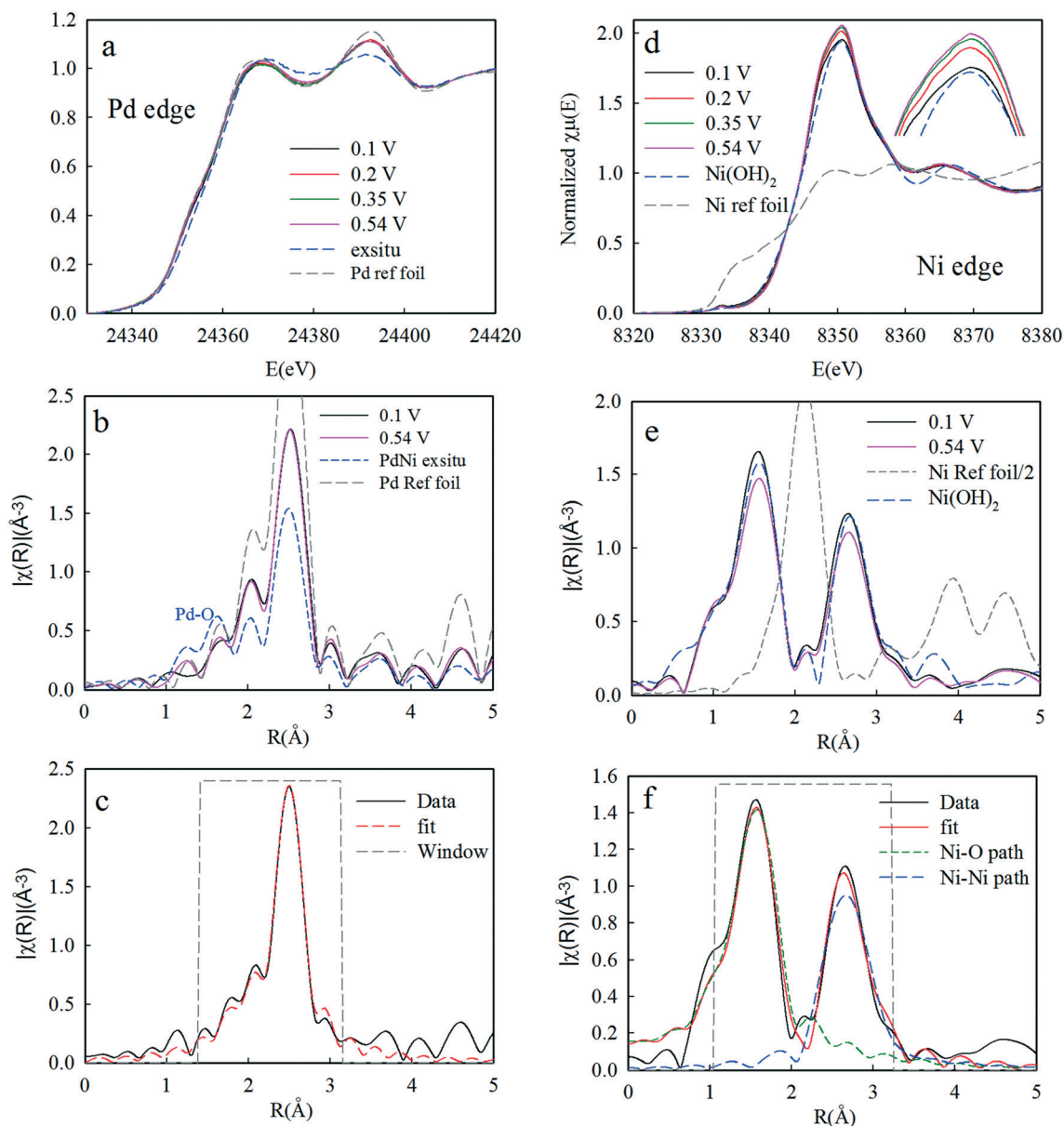
This journal is © The Royal Society of Chemistry 2021

Catal. Sci. Technol., 2021, **11**, 1337–1344 | **1341**

Fig. 5 The *ex situ* and *in situ* XANES spectra at the Pd (a) and Ni (d) edges; the *in situ* FT-EXAFS spectra at the Pd (b) and Ni (e) edges; and the EXAFS fitting of the Pd (c) and Ni (f) edges of Pd/γ-NiOOH.

Table 1 Summary of the EXAFS fitting results of Pd/γ-NiOOH at 0.1 V_{RHE} in an H_2-saturated 0.1 M KOH electrolyte[a]

Pd edge	R (Å)	N	$\sigma^2 \times 10^{-3}$ (Å^2)	E_0
Pd–Pd	2.738 ± 0.003	10.3 ± 0.5	0.007 ± 0.001	−1.1 ± 0.3
Pd foil	2.737 ± 0.002	12	0.006 ± 0.001	0.4 ± 0.3
Ni edge	R (Å)	N	$\sigma^2 \times 10^{-3}$ (Å^2)	E_0
Ni–O	2.08 ± 0.02	6.3 ± 0.9	0.007 ± 0.003	−1.1 ± 1.5
Ni–Ni	3.08 ± 0.01	6.4 ± 1.9		

[a] Fits were done separately at the Pd and Ni K-edges in R-space, $k^{1,2,3}$ weighting. 1.38 < R < 3.13 Å and Δk = 3.00–13.61 Å^{-1} were used for fitting the Pd K-edge data; 1.1 < R < 3.3 Å and Δk = 2.46–9.65 Å^{-1} were used for fitting the Ni K-edge data. S_0^2 was fixed at 0.797 for Pd edge and 0.75 for Ni edge obtained by fitting the corresponding reference foil.

the oxidation of Ni. This reversible trend indicates that the surface Ni oxy-hydroxides are redox active within the HOR kinetic potential region. This redox behavior is believed to facilitate the generation of adsorbed hydroxyl (OH_{ad}),[34] and thus favors the bifunctional mechanism wherein the OH_{ad} hosted by Ni oxides facilitates the oxidative removal of H_{ad} on the adjacent Pd site, thereby promoting the HOR.[35,36] On the other hand, the enhancement observed with the additional NiOOH phase on Pd is also in agreement with the enhancement observed on Pt/Ni(OH)$_2$ surfaces, where Ni(OH)$_2$ clusters promote the hydrogen evolution rate by lowering the interfacial water reorganization in alkaline medium.[37]

4. Conclusions

In summary, we have reported on the organometallic synthesis of high-surface-area carbon supported Pd/γ-NiOOH HOR electrocatalyst. The 2 nm cubic nanocrystals of nickel oxyhydroxide (γ-NiOOH) grow selectively on the Pd surface with a 20% coverage, which leads to an optimal electrochemical surface area ratio of 1:1 between the two phases. The 10-fold increase in exchange current density and a 5-fold increase in mass activity is attributed to the formation of this novel oxophilic phase. *Operando* X-ray absorption spectroscopy on a catalyst layer reveals the redox activity of Pd and Ni active surface sites during the electrocatalysis. Undoubtedly, each phase has a given role in the mechanism, hydrogen binding to the Pd metal and hydroxide binding to the γ-NiOOH, confirming the theory and experiments observed on Pd/Ni bimetallic films and dispersed catalysts.

Conflicts of interest

The authors declare no competing financial interest.

Acknowledgements

Notes and references

1 S. Lu, J. Pan, A. Huang, L. Zhuang and J. Lu, Alkaline polymer electrolyte fuel cells completely free from noble metal catalysts, *Proc. Natl. Acad. Sci. U. S. A.*, 2008, **105**, 20611–20614, DOI: 10.1073/PNAS.0810041106.

2 J. R. Varcoe, P. Atanassov, D. R. Dekel, A. M. Herring, M. A. Hickner, P. A. Kohl, A. R. Kucernak, W. E. Mustain, K. Nijmeijer, K. Scott, T. Xu and L. Zhuang, Anion-exchange membranes in electrochemical energy systems, *Energy Environ. Sci.*, 2014, **7**, 3135–3191, DOI: 10.1039/C4EE01303D.

3 S. Gottesfeld, D. R. Dekel, M. Page, C. Bae, Y. Yan, P. Zelenay and Y. S. Kim, Anion exchange membrane fuel cells: Current status and remaining challenges, *J. Power Sources*, 2018, **375**, 170–184, DOI: 10.1016/j.jpowsour.2017.08.010.

4 A. Serov, I. V. Zenyuk, C. G. Arges and M. Chatenet, Hot topics in alkaline exchange membrane fuel cells, *J. Power Sources*, 2018, **375**, 149–157, DOI: 10.1016/j.jpowsour.2017.09.068.

5 N. M. Markovic, H. A. Gasteiger and P. N. Ross, Oxygen Reduction on Platinum Low-Index Single-Crystal Surfaces in Sulfuric Acid Solution: Rotating Ring-Pt(hkl) Disk Studies, *J. Phys. Chem.*, 2002, **99**, 3411–3415, DOI: 10.1021/j100011a001.

6 W. Sheng, H. A. Gasteiger and Y. Shao-Horn, Hydrogen Oxidation and Evolution Reaction Kinetics on Platinum: Acid vs Alkaline Electrolytes, *J. Electrochem. Soc.*, 2010, **157**, B1529, DOI: 10.1149/1.3483106.

7 P. Rheinlander, S. Henning, J. Herranz and H. A. Gasteiger, Comparing Hydrogen Oxidation and Evolution Reaction Kinetics on Polycrystalline Platinum in 0.1 M and 1 M KOH, *ECS Trans.*, 2013, **50**, 2163–2174, DOI: 10.1149/05002.2163ecst.

8 J. Durst, A. Siebel, C. Simon, F. Hasché, J. Herranz and H. A. Gasteiger, New insights into the electrochemical hydrogen oxidation and evolution reaction mechanism, *Energy Environ. Sci.*, 2014, **7**, 2255–2260, DOI: 10.1039/C4EE00440J.

9 H. Wang and H. D. Abruña, IrPdRu/C as H2 Oxidation Catalysts for Alkaline Fuel Cells, *J. Am. Chem. Soc.*, 2017, **139**, 6807–6810, DOI: 10.1021/jacs.7b02434.

10 R. Subbaraman, D. Tripkovic, D. Strmcnik, K.-C. Chang, M. Uchimura, A. P. Paulikas, V. Stamenkovic and N. M. Markovic, Enhancing Hydrogen Evolution Activity in Water Splitting by Tailoring Li+-Ni(OH)2-Pt Interfaces, *Science*, 2011, **334**, 1256–1260, DOI: 10.1126/science.1211934.

11 R. Subbaraman, N. Danilovic, P. P. Lopes, D. Tripkovic, D. Strmcnik, V. R. Stamenkovic and N. M. Markovic, Origin of Anomalous Activities for Electrocatalysts in Alkaline Electrolytes, *J. Phys. Chem. C*, 2012, **116**, 22231–22237, DOI: 10.1021/jp3075783.

12 W. Sheng, A. P. Bivens, M. Myint, Z. Zhuang, R. V. Forest, Q. Fang, J. G. Chen and Y. Yan, Non-precious metal electrocatalysts with high activity for hydrogen oxidation reaction in alkaline electrolytes, *Energy Environ. Sci.*, 2014, **7**, 1719–1724, DOI: 10.1039/C3EE43899F.

13 A. Manzo-Robledo, N. J. S. Costa, K. Philippot, L. M. Rossi, E. Ramírez-Meneses, L. P. A. Guerrero-Ortega and S. Ezquerra-Quiroga, Electro-oxidation of methanol in alkaline conditions using Pd–Ni nanoparticles prepared from organometallic precursors and supported on carbon vulcan, *J. Nanopart. Res.*, 2015, **17**, 474, DOI: 10.1007/s11051-015-3287-8.

14 T. Mikolajczyk, M. Turemko and B. Pierozynski, Ethanol oxidation reaction at Pd-modified nickel foam obtained by

This journal is © The Royal Society of Chemistry 2021

Catal. Sci. Technol., 2021, **11**, 1337–1344 | **1343**

PVD method in alkaline solution, *J. Electroanal. Chem.*, 2014, **735**, 32–35, DOI: 10.1016/j.jelechem.2014.10.003.

15 A. Zadick, L. Dubau, K. Artyushkova, A. Serov, P. Atanassov and M. Chatenet, Nickel-based electrocatalysts for ammonia borane oxidation: enabling materials for carbon-free-fuel direct liquid alkaline fuel cell technology, *Nano Energy*, 2017, **37**, 248–259, DOI: 10.1016/j.nanoen.2017.05.035.

16 E. S. Davydova, S. Mukerjee, F. Jaouen and D. R. Dekel, Electrocatalysts for Hydrogen Oxidation Reaction in Alkaline Electrolytes, *ACS Catal.*, 2018, **8**, 6665–6690, DOI: 10.1021/acscatal.8b00689.

17 M. Shao, Palladium-based electrocatalysts for hydrogen oxidation and oxygen reduction reactions, *J. Power Sources*, 2011, **196**, 2433–2444, DOI: 10.1016/j.jpowsour.2010.10.093.

18 W. Sheng, M. Myint, J. G. Chen and Y. Yan, Correlating the hydrogen evolution reaction activity in alkaline electrolytes with the hydrogen binding energy on monometallic surfaces, *Energy Environ. Sci.*, 2013, **6**, 1509–1512, DOI: 10.1039/C3EE00045A.

19 I. Bakos, A. Paszternák and D. Zitoun, Pd/Ni Synergestic Activity for Hydrogen Oxidation Reaction in Alkaline Conditions, *Electrochim. Acta*, 2015, **176**, 1074–1082, DOI: 10.1016/j.electacta.2015.07.109.

20 M. Alesker, M. Page, M. Shviro, Y. Paska, G. Gershinsky, D. R. Dekel and D. Zitoun, Palladium/nickel bifunctional electrocatalyst for hydrogen oxidation reaction in alkaline membrane fuel cell, *J. Power Sources*, 2016, **304**, 332–339, DOI: 10.1016/j.jpowsour.2015.11.026.

21 N. J. S. Costa, M. Guerrero, V. Collière, É. Teixeira-Neto, R. Landers, K. Philippot and L. M. Rossi, Organometallic Preparation of Ni, Pd, and NiPd Nanoparticles for the Design of Supported Nanocatalysts, *ACS Catal.*, 2014, **4**, 1735–1742, DOI: 10.1021/cs500337a.

22 M. Shviro, S. Polani, R. E. Dunin-Borkowski and D. Zitoun, Bifunctional Electrocatalysis on Pd-Ni Core–Shell Nanoparticles for Hydrogen Oxidation Reaction in Alkaline Medium, *Adv. Mater. Interfaces*, 2018, **5**, 1–8, DOI: 10.1002/admi.201701666.

23 M. Shviro, A. Paszternák, A. Chelly and D. Zitoun, Zigzag-shaped nickel nanowires via organometallic template-free route, *J. Nanopart. Res.*, 2013, **15**, 1823, DOI: 10.1007/s11051-013-1823-y.

24 M. Shviro and D. Zitoun, Low temperature, template-free route to nickel thin films and nanowires, *Nanoscale*, 2012, **4**, 762–767, DOI: 10.1039/c1nr11177a.

25 M. Shviro and D. Zitoun, Nickel nanocrystals: fast synthesis of cubes, pyramids and tetrapods, *RSC Adv.*, 2013, **3**, 1380, DOI: 10.1039/c2ra22024e.

26 H. A. Miller, A. Lavacchi, F. Vizza, M. Marelli, F. Di Benedetto, F. D'Acapito, Y. Paska, M. Page and D. R. Dekel, A Pd/C-CeO2Anode Catalyst for High-Performance Platinum-Free Anion Exchange Membrane Fuel Cells, *Angew. Chem., Int. Ed.*, 2016, **55**, 6004–6007, DOI: 10.1002/anie.201600647.

27 H. A. Miller, F. Vizza, M. Marelli, A. Zadick, L. Dubau, M. Chatenet, S. Geiger, S. Cherevko, H. Doan, R. K. Pavlicek, S.

Mukerjee and D. R. Dekel, Highly active nanostructured palladium-ceria electrocatalysts for the hydrogen oxidation reaction in alkaline medium, *Nano Energy*, 2017, **33**, 293–305, DOI: 10.1016/j.nanoen.2017.01.051.

28 T. J. Omasta, X. Peng, H. A. Miller, F. Vizza, L. Wang, J. R. Varcoe, D. R. Dekel and W. E. Mustain, Beyond 1.0 W cm $^{-2}$ Performance without Platinum: The Beginning of a New Era in Anion Exchange Membrane Fuel Cells, *J. Electrochem. Soc.*, 2018, **165**, J3039–J3044, DOI: 10.1149/2.0071815jes.

29 V. Yarmiayev, M. Alesker, A. Muzikansky, M. Zysler and D. Zitoun, Enhancement of Palladium HOR Activity in Alkaline Conditions through Ceria Surface Doping, *J. Electrochem. Soc.*, 2019, **166**, F3234–F3239, DOI: 10.1149/2.0291907jes.

30 H. Yu, E. S. Davydova, U. Ash, H. A. Miller, L. Bonville, D. R. Dekel and R. Maric, Palladium-ceria nanocatalyst for hydrogen oxidation in alkaline media: Optimization of the Pd–CeO2 interface, *Nano Energy*, 2019, **57**, 820–826, DOI: 10.1016/j.nanoen.2018.12.098.

31 Z. Tatus-Portnoy, A. Kitayev, T. V. Vineesh, E. Tal-Gutelmacher, M. Page and D. Zitoun, A low-loading Ru-rich anode catalyst for high-power anion exchange membrane fuel cells, *Chem. Commun.*, 2020, 5669–5672.

32 T. M. Arruda, B. Shyam, J. S. Lawton, N. Ramaswamy, D. E. Budil, D. E. Ramaker and S. Mukerjee, Fundamental aspects of spontaneous cathodic deposition of Ru onto Pt/C electrocatalysts and membranes under direct methanol fuel cell operating conditions: An in situ X-ray absorption spectroscopy and electron spin resonance study, *J. Phys. Chem. C*, 2010, **114**, 1028–1040, DOI: 10.1021/jp908082j.

33 Q. Jia, W. Liang, M. K. Bates, P. Mani, W. Lee and S. Mukerjee, Activity descriptor identification for oxygen reduction on platinum-based bimetallic nanoparticles: In situ observation of the linear composition-strain-activity relationship, *ACS Nano*, 2015, **9**, 387–400, DOI: 10.1021/nn506721f.

34 R. Subbaraman, D. Tripkovic, K. C. Chang, D. Strmcnik, A. P. Paulikas, P. Hirunsit, M. Chan, J. Greeley, V. Stamenkovic and N. M. Markovic, Trends in activity for the water electrolyser reactions on 3d M(Ni,Co,Fe,Mn) hydr(oxy)oxide catalysts, *Nat. Mater.*, 2012, **11**, 550–557, DOI: 10.1038/nmat3313.

35 D. Strmcnik, M. Uchimura, C. Wang, R. Subbaraman, N. Danilovic, D. van der Vliet, A. P. Paulikas, V. R. Stamenkovic and N. M. Markovic, Improving the hydrogen oxidation reaction rate by promotion of hydroxyl adsorption, *Nat. Chem.*, 2013, **5**, 300–306, DOI: 10.1038/nchem.1574.

36 J. Li, S. Ghoshal, M. K. Bates, T. E. Miller, V. Davies, E. Stavitski, K. Attenkofer, S. Mukerjee, Z.-F. Ma and Q. Jia, Experimental Proof of the Bifunctional Mechanism for the Hydrogen Oxidation in Alkaline Media, *Angew. Chem., Int. Ed.*, 2017, **56**, 15594–15598, DOI: 10.1002/anie.201708484.

37 I. Ledezma-Yanez, W. D. Z. Wallace, P. Sebastián-Pascual, V. Climent, J. M. Feliu and M. T. M. Koper, Interfacial water reorganization as a pH-dependent descriptor of the hydrogen evolution rate on platinum electrodes, *Nat. Energy*, 2017, **2**, 1–7, DOI: 10.1038/nenergy.2017.31.